

ADVANCES IN AEROTHERMAL MODELING FOR TMT

Konstantinos Vogiatzis
TMT Observatory Corp., Pasadena, CA, USA

ABSTRACT

The performance requirements of the Thirty Meter Telescope (TMT) dictate, among others, a thorough understanding of the flow field inside and around the observatory. Mirror and dome seeing as well as dynamic wind loading on the optics, telescope structure and enclosure constitute significant sources of image degradation. A summary of the current status of Computational Fluid Dynamics (CFD) simulations for TMT is presented, with special attention given to the choice of thermal boundary conditions.

Detailed simulations of the mirror support assemblies determine the direction of heat flow from important heat sources and provide feedback to the design. They also provide estimates of the heat transfer coefficients for the solid thermal models.

A transient radiation model has also been developed for the enclosure and telescope surfaces in order to estimate the heat flux exchange with the air volume. It also provides estimates of the effective emissivity for the solid thermal models.

Finally, a complete model of the observatory on a candidate summit is used to calculate air velocity, pressure and temperature for a matrix of given telescope orientations and enclosure configurations. Calculated wind velocity spectra above M1 and around M2 as well as the wind force on the enclosure are used as inputs in the TMT integrated dynamic model. The temperature and flux output of the aforementioned thermal models are used as input surface boundary conditions in the CFD model. Generated records of temperature variations inside the air volume of the optical paths are fed into the TMT thermal seeing model.

Keywords: Extremely Large Telescopes, Thermal and Aerodynamic Modeling, Computational Fluid Dynamics

1. INTRODUCTION

Wind and temperature are fundamental environmental parameters influencing the performance of large ground-based telescopes. Wind buffeting, mirror and enclosure local seeing are aspects of medium (air) induced image degradation that are very hard to estimate without the use of numerical simulations. Moreover, even in the absence of medium, thermal effects could become important due to radiation.

Computational Fluid Dynamics (CFD) techniques have come a long way since the first attempt to simulate the flow field inside and around a 30m-class telescope [1]. The evolution of the design of the Thirty Meter Telescope (TMT), both in detail and in innovation, provides the challenge for a corresponding evolution of modeling, for performance estimates and design feedback [2], [3]. In this study we present the advances recently achieved in aero-thermal modeling for TMT. Ideally, aero-thermal modeling should involve a combined solid and fluid grid with conjugate heat transfer (conduction and convection), radiation and air turbulence solvers. At every time-step the grid would be modified according to the telescope/enclosure orientation, the environmental (ambient boundary) conditions would change, the temperature field and wind forces on the telescope structure would be obtained, incorporated wind buffeting and ray-tracing models would solve for dynamic and thermal seeing and a performance metric would be calculated. The time-steps could span a record of observed environmental conditions. Unfortunately the time when this can be possible has yet to arrive. But based on current computational power and we can do the next best thing.

Figure 1 depicts the current TMT aero-thermal modeling synergy. The gray box called “Standard Year” is the TMT Monte Carlo Simulation Framework [4] and, besides mirror seeing, fuses together performance estimates for optical surface shapes, wind seeing and dome seeing. It utilizes the PSS performance metric [5]. A two-year environmental record measured on the TMT baseline site [6] provides ambient condition variability. The Segment Support Assembly (SSA) CFD model provides heat transfer coefficients to the SSA solid thermal model [7], which in turn provides heat fluxes to the mirror thermal model. The surface thermal model provides heat fluxes to the TMT observatory CFD model. It can also provide the solid thermal models (SSA and mirror [4]) with correct radiation properties. The convective heat transfer coefficients needed by the surface model are provided by isothermal CFD simulations. The thermal CFD simulations yield velocity and temperature field used by the wind [8] and dome seeing [9] models respectively.

In the following sections we will present the SSA CFD model, the surface thermal model and the current TMT Observatory model, along with a compilation of representative results.

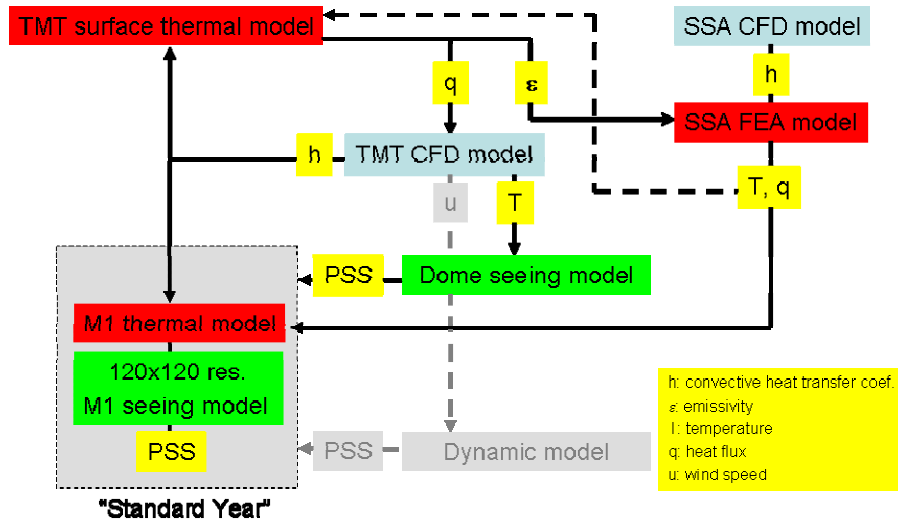


Figure 1. TMT aero-thermal modeling synergy

2. LOCAL CFD MODELS

SSA simulation

The most characteristic example of local CFD models is the SSA model. Figure 2 shows the current TMT SSA assembly and the corresponding CFD model.

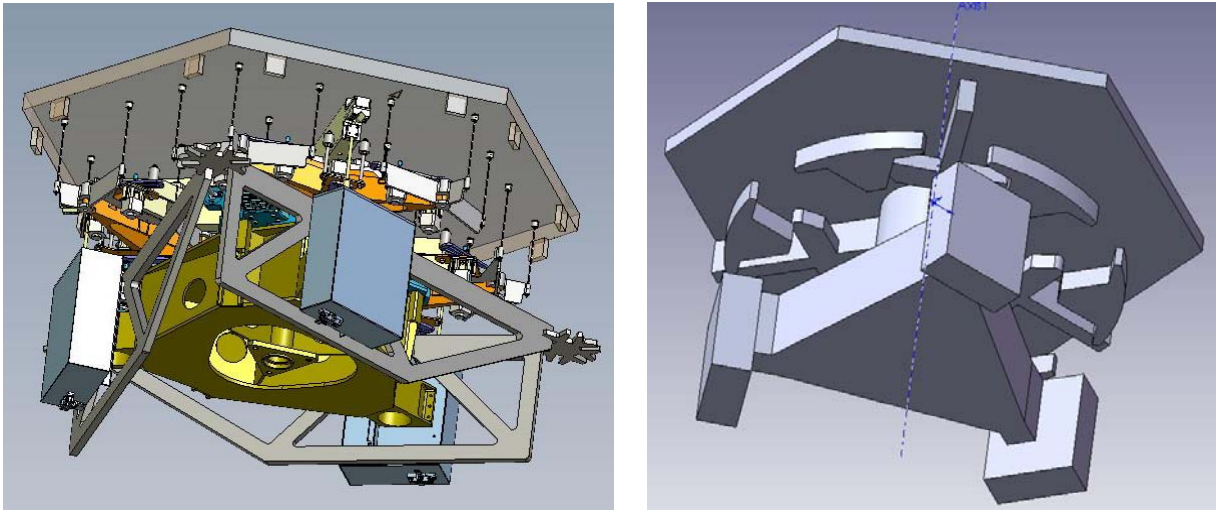


Figure 2. SSA design (left) and CFD model (right)

2.1 Actuator heat dissipation

Since the solid thermal model described in [7] models also the edge sensor preamplifiers the resulting heat flux from those sources need not be modeled. However, the solid thermal model requires the convective heat transfer coefficient as input. This number is provided by the CFD simulation and is of order $1\text{W/m}^2/\text{K}$ for the mirror back surface. Moreover, the solid model does not take into account the change in the ambient air temperature from the heat dissipated by the actuators into the shielded environment. Therefore the additional heat flux on the mirror surface caused by the actuator plumes is modeled in this simulation. The actuator surfaces will be $\sim 0.7\text{K}$ above ambient temperature [7]. Figure 3 shows the resulting heat flux with the above boundary condition. Most of the surface receives less than 0.3W/m^2 with only very small areas having an influx of $\sim 1\text{W/m}^2$.

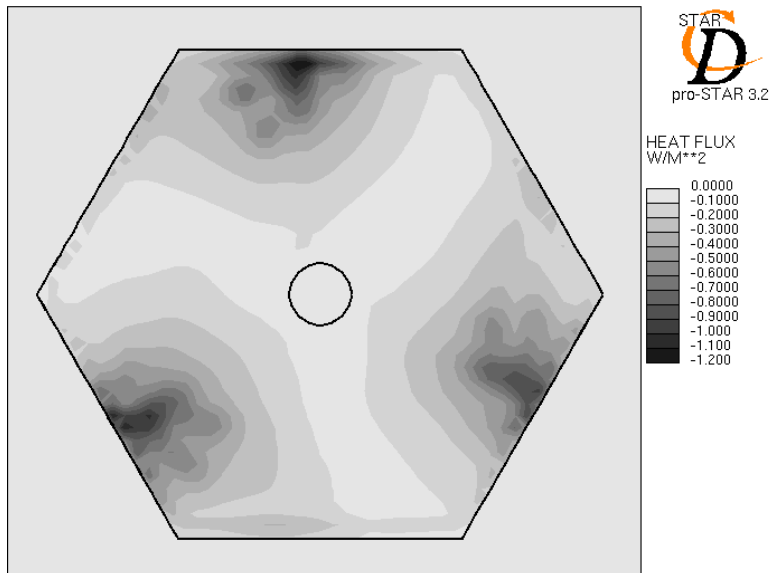


Figure 3. Heat flux into the back of a segment caused by actuator plumes
(Negative values denote heat loss for the fluid, thus heat gain for the solid surface)

3. THERMAL MODELS

Surface thermal model

Proper thermal boundary conditions on the enclosure surfaces are important for correctly capturing the temperature field inside the optical path. In places where the wind speed is low the temperature gradients on the surfaces cannot be contained close to them since diffusion and buoyancy dominate. Also as the wind moves over the area around the enclosure aperture, the exterior surface temperature introduces a gradient which then passes through the optical path. In order to estimate the correct heat flux on the enclosure surfaces a model that takes into account the constant movement of the enclosure components, convection and, most importantly, radiation, was implemented. It can also provide information on surface temperature spatial gradients and temperature ranges for specific locations or components. It can estimate the limits on heat dissipation for specific components. Finally, it can estimate the daytime Ac power requirement due to solar radiation and other interior heat sources.

3.1 Methodology

Figure 4 depicts the geometry of the enclosure exterior/interior and the telescope components resolved. The enclosure surfaces are divided into floor, fixed base, rotating base, cap, three vent layers and aperture. The cap and the rotating base can move independently. The components resolved include the primary mirror and its support platform, the M2 assembly, M3, the rockers and some instruments as reference volumes. Apart from M1, the telescope components do not alter the radiation results, but they can be used to track their local temperatures. The aperture and the vents (when open) are treated as black bodies and assume the sky or ground temperature depending on viewing angle. Solid surface elements retain their thickness, while closed surface components are assigned surface thicknesses to match their weight. The interior surface elements are approximately 3,500 and the exterior 1,300. Another 800 elements form the ground and the sky.

The lumped mass temperature tracking model is joined by a convection model that uses CFD heat transfer coefficient maps for various orientations and a radiosity model, which estimates the apparent emissivity of each element or, in other words, the net radiation flux after all emissions and reflections are accounted for.

The model uses as input the same record of environmental parameters (wind and temperature) and telescope orientations as presented in [4]. At each time-step the enclosure components move according to the current orientation, the view factors and radiosity are calculated, the convection heat flux term is added and the thermal balance equation is solved. The effective sky temperature and daytime insolation vary with the zenith angle. A fixed grid would yield low accuracy results especially for the cap surface elements, the centroid of which exhibits a significant range in elevation. The great advantage of this model against any existing (in house or commercial) radiation model is that the view factors are

updated at every step, making it a true transient analysis. This approach has been used in the animation industry to create the proper lighting effects.

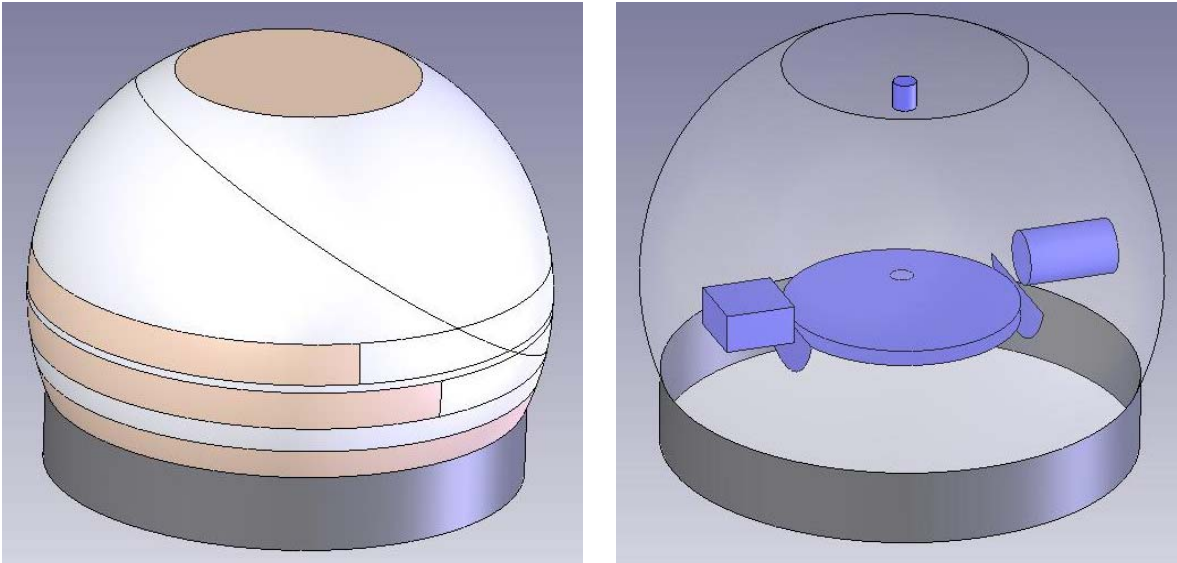


Figure 4. Enclosure (left) and telescope component (right) model geometry

3.2 Representative results

A simulation that used a time record of ambient temperatures and telescope orientations for an entire night was conducted. Figure 5 shows the average net heat flux on the interior enclosure surfaces (telescope components excluded) as a function of time after sunset. The interior surfaces emissivity was set to 0.5. Right after sunset the enclosure surfaces gain heat as the air temperature is warmer and they were kept cool during the day. But soon enough radiation takes over and the average heat loss for the night is -1.6W/m^2 . Note the abrupt change 2h after sunset, when the wind slowed down and the vents opened to add more area, through which the enclosure could radiate to the sky.

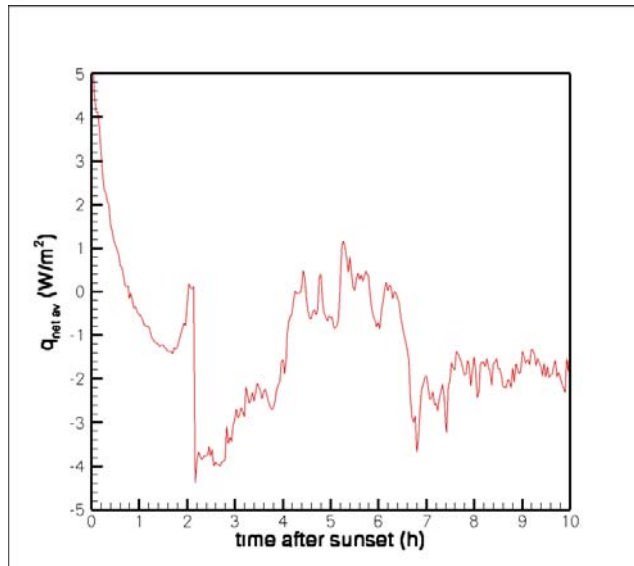


Figure 5. Average net heat flux for the interior enclosure surface as a function of time after sunset

In Figure 6 the temperature behavior of the exterior surface around the aperture after sunset is presented. The exterior surface emissivity was set to 0.9. Assuming that the surface temperature is the same with the ambient at sunset, the

exterior skin of the enclosure can cool down by 6K and maintain that temperature difference throughout the night. In reality the skin temperature will still be higher than ambient from the daytime heat, so the radiation effect will not be that pronounced. The model can be used to select a particular exterior paint that optimizes the trade between daytime air-conditioning and night-time temperature gradients that affect the optical path.

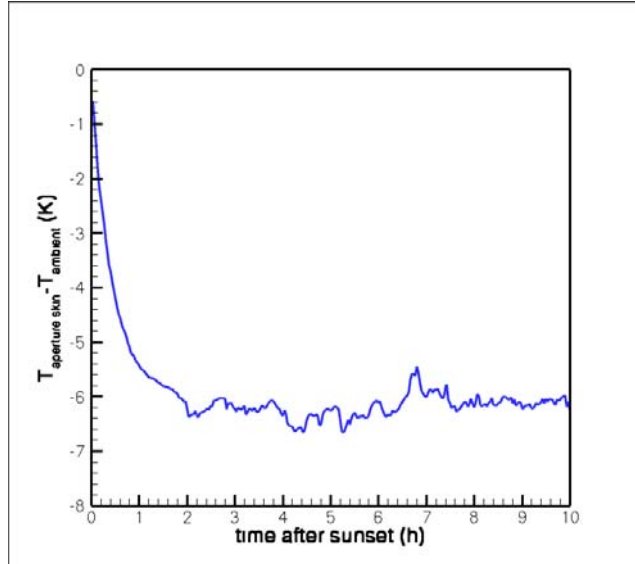


Figure 6. Temperature difference between the exterior enclosure skin close to the aperture and ambient temperature as a function of time after sunset

4. OBSERVATORY CFD MODEL

General configuration

The general set-up for CFD simulations has been extensively reported in earlier work [1], [2], [3]. We will focus here on the enhancements-updates. Figure 7 shows the latest TMT enclosure and telescope design resolved by CFD. The Calotte enclosure is placed on the baseline TMT summit and facility buildings have been incorporated. The summit has a 5m resolution while the enclosure and telescope grids have a horizontal surface resolution of 0.5m-1m and a surface thickness resolution of 0.05m-0.1m. Features that do not affect the flow aerodynamically or thermally and are less than 1m in diameter have been omitted. The computational domain is 15x15x5 in dome diameter units.

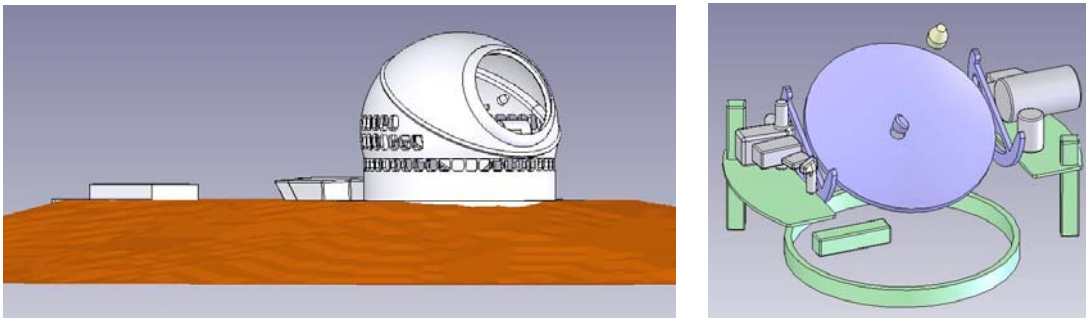


Figure 7. TMT Observatory CFD model (left) and the telescope model placed inside (right)

18 different orientations have been investigated, with three different zenith angles ($0^\circ - 32.5^\circ - 65^\circ$), three different relative to wind azimuth angles ($0^\circ - 90^\circ - 180^\circ$) and vents being fully open or fully closed. The relative to wind azimuth angle is defined by the wind direction and the telescope plane normal to the elevation axis. Most of the cases used a north absolute wind direction and a few used south. These are the two prevailing baseline site wind directions (75%-

25%) [6]. Air properties have been taken at ~3000m. The temperature vertical gradient is set to -6K/km above 100m (from balloon measurements) and the ground heat flux is set to -40W/m² (from SODAR flux gauge). For the closed vents cases the reference wind speed at 20m is 10m/s and for the open vent cases is 3m/s. In both cases the average resulting wind speed above the primary mirror is ~1m/s, which is equal to the TMT M1 target velocity [8] (see appendix for vent operating strategy).

The CFD simulations performed with this configuration can be grouped into two categories, steady state and transient (unsteady).

4.1 TMT observatory – steady state simulations

They provide the wind reduction factors for telescope top end and segment wind buffeting in the form of mean and rms velocities, normalized with the reference wind speed. They also provide information on venting efficiency for mirror flushing and enclosure volume exchange. Convective heat transfer coefficient maps on M1 and on the enclosure surfaces are also provided for use in the mirror and surface thermal models respectively. Finally the simulations are used to provide feedback to summit development design

4.1.1 Top-end loading

Figure 8 shows a representative contour plot of the wind reduction factor on a plane normal to the elevation axis. The configuration is zenith 32.5°, azimuth 0° (facing north), closed vents, reference north wind speed 10m/s. The wind speed experienced by the top end of the telescope is less than 10% of the external. The TMT enclosure has been optimized for this zenith region, since it is expected to be the median telescope orientation.

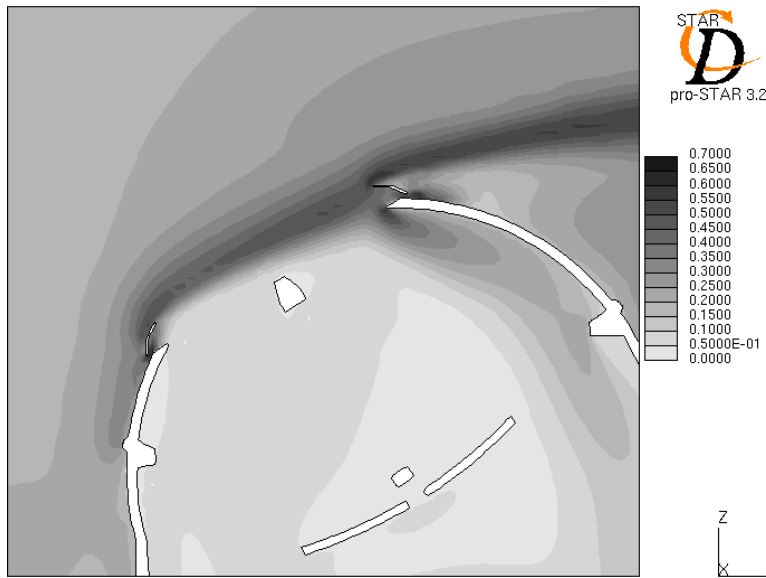


Figure 8. Wind reduction factor contour plot on a plane normal to the elevation axis, flow from the left, za=32.5°, az=0°, closed vents, 10m/s

4.1.2 M1 heat transfer

Figure 9 shows a representative contour plot of the convective heat transfer coefficient on M1 surface. The configuration is zenith 0°, closed vents, reference north wind speed 10m/s. On the right, the corresponding wind speed above M1. Even though the average wind speed does not exceed 0.3m/s, turbulent mixing yields an average coefficient of at least 4W/m²/K, which is adequate for mirror cooling. At the same time the segments do not suffer significant buffeting.

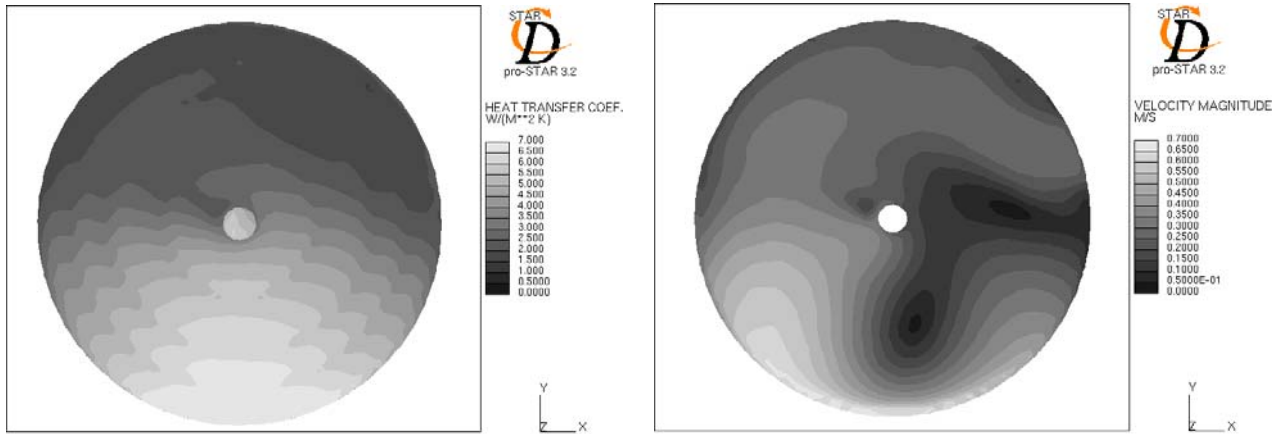


Figure 9. Heat transfer coefficient contour on M1 (left) and corresponding mean velocity (right), flow from above, $z_a=0^\circ$, $z_z=0^\circ$, closed vents, 10m/s

4.1.3 Dome flushing

The inherent venting asymmetry of the Calotte design prompts us to investigate particular orientations for adequate enclosure flushing. One such orientation is zenith 32.5° , relative to wind azimuth 90° . In this case the well vented side of the enclosure is upwind but there is no flow-through since the un-vented cap is downwind, as depicted in Figure 10. We release air “particles” along the optical path (between M3 and M2) and track them for several minutes. After 2min 80% of them have exited the enclosure through the aperture and the rest have impinged on the cap interior (that does not mean they are stagnant but the program does not follow them further). So, even in this orientation and wind speed (3m/s), there will be volume exchange in short time-scales at the expense of added turbulence along the optical path.

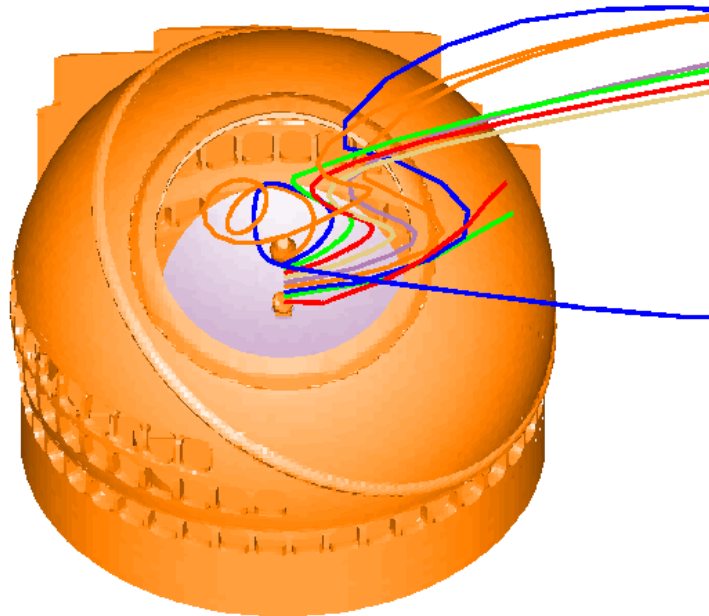


Figure 10. Particle tracking for enclosure volume exchange, flow from the left, $z_a=32.5^\circ$, $z_z=90^\circ$, open vents, 3m/s

4.2 TMT observatory – unsteady simulations

These simulations are useful for high order wind and thermal behavior. Temperature records inside the optical path are provided to the dome seeing model. Velocity and pressure records and spectra on the telescope or the enclosure exterior surfaces can be used in the wind buffeting model.

4.2.1 Optical turbulence

One-minute long temperature records along the optical path from the primary mirror surface up to ~20m past the enclosure aperture are generated at 1Hz sampling rate and fed to the dome seeing model [9]. Figure 11 shows representative snapshots of the temperature field on the plane defined by the elevation axis and the optical axis and above the M1 surface. The configuration is again zenith 32.5° , relative to wind azimuth 90° , open vents, 3m/s. The reference temperature at 20m is 282K.

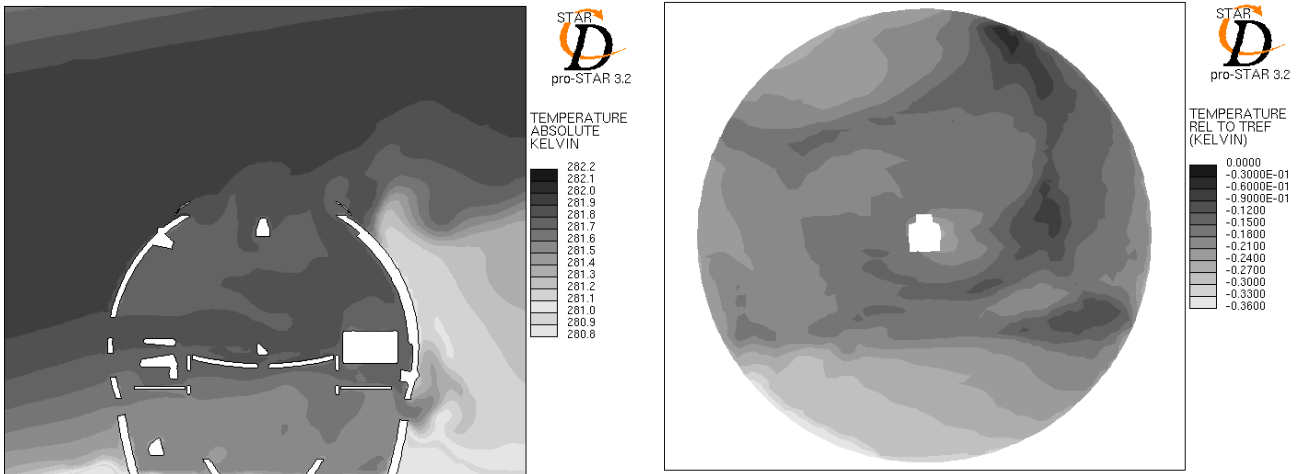


Figure 11. Temperature contour plot on a plane defined by the elevation axis and the optical axis (left) and above M1 surface (right), flow from the left, $z_a=32.5^\circ$, $az=90^\circ$, open vents, 3m/s, $T_{REF} = 282K$

4.2.2 M1 loading

Velocity time records can be obtained for locations above M1 and can provide spectra to be used in the integrated dynamic model for segment loading.

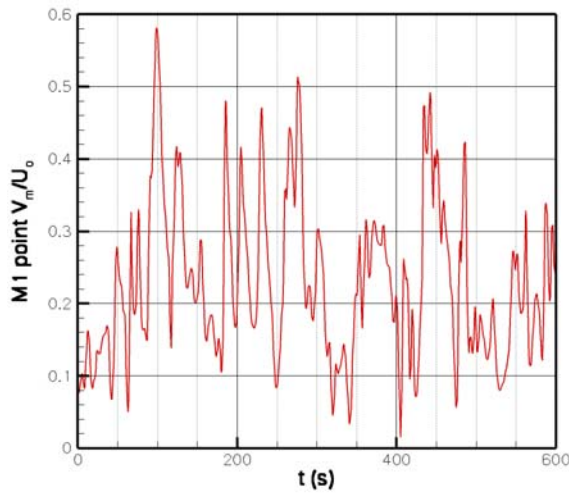


Figure 12. Normalized velocity on an M1 point, $z_a=32.5^\circ$, $az=0^\circ$, open vents, 5m/s

A representative time record of mean wind speed normalized with the external wind speed of 5m/s at 1Hz for a period of 10min is plotted in Figure 12. The configuration is zenith 32.5° , relative to wind azimuth 0° , open vents. The mean wind speed on M1 is $\sim 1.2\text{m/s}$. The same information of course can also be obtained for the top end of the telescope.

4.2.3 Enclosure loading

Finally, pressure records have been obtained from the enclosure exterior surface. The configuration for this simulation is zenith 32.5° , relative to wind azimuth 0° , closed vents, 10m/s. The sampling rate is 5Hz and the record is 1min long. The pressures were integrated along the enclosure surface and the center of pressure was found to be 20m from the ground (3m below the elevation axis). The parallel to flow (drag), normal to flow (Karman shedding) and normal to ground (lift) forces were also estimated. Figure 13 has the resulting force time record, along with a snapshot of pressure variations on a plane parallel to the ground at the center of pressure level. The frequency of the Karman shedding is accurately captured at $\sim 0.042\text{Hz}$ (Strouhal number for very high Re numbers is ~ 0.25 , reference wind speed is 10m/s and reference diameter is $\sim 60\text{m}$ at the level of center of pressure). The distance between two vortices is around 240m (black line), which is approximately the distance covered by a vortex at 10m/s in one period. It is clear that the Karman shedding force is the largest contributor to unsteady enclosure forces, being around 20kN, while its mean is not exactly zero (7.4kN) due to the enclosure geometric asymmetries. Mean drag is 48.1kN, resulting in an aerodynamic coefficient of 0.3. Its dynamic component is small and as expected at double the Karman frequency. Finally the mean lift is considerable at 58.9kN but with almost no dynamic component. The forces are fed into an enclosure-soil-pier interaction model [10] to assess the importance of enclosure forces in image jitter.

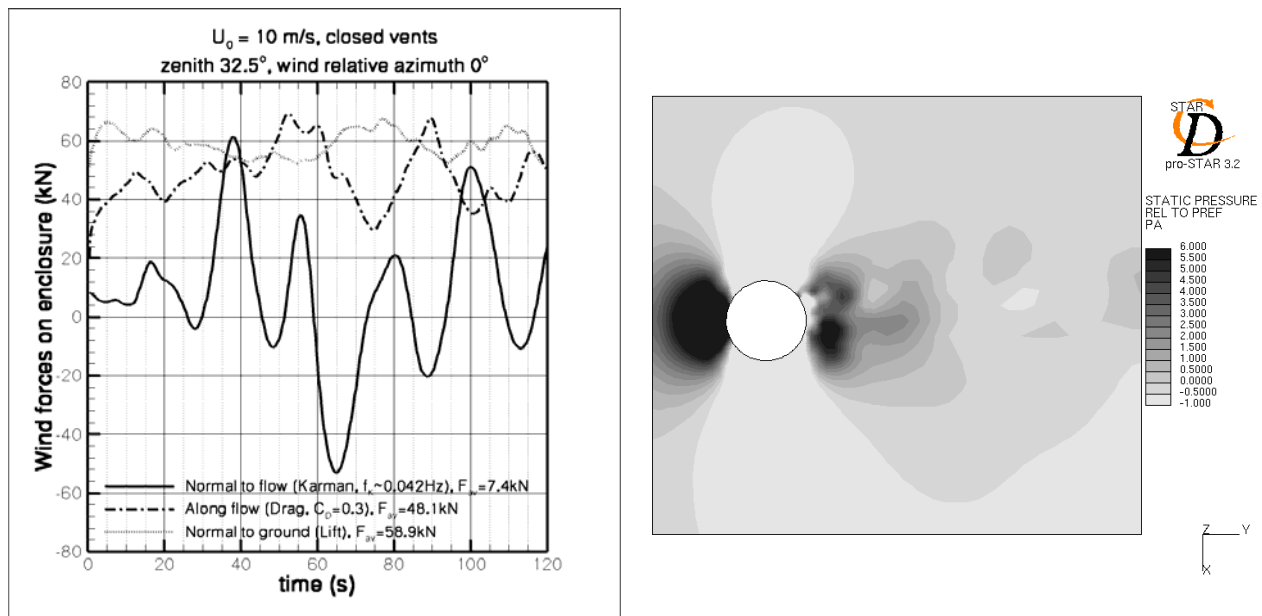


Figure 13. Record of enclosure forces (left) and pressure snapshot (right), $z_a=32.5^\circ$, $z_a=0^\circ$, closed vents, 10m/s

5. CONCLUSIONS

The brief overview of results presented here provides only a sample of the capabilities available through the current thermal models and CFD simulations of wind flow around and inside enclosure-telescope configurations for the next generation of extremely large telescopes. We have created an aero-thermal modeling framework that provides a range of inputs to a group of performance estimate models utilized by the TMT Systems Engineering team. We will continue to enhance these models as well as develop new ones, in order to meet the ever growing need for design guidance and performance analysis.

ACKNOWLEDGMENTS

The author would like to thank Myung Cho (NOAO) for his contribution in understanding the thermal environment of the TMT primary mirror.

The author gratefully acknowledges the support of the TMT partner institutions. They are the Association of Canadian Universities for Research in Astronomy (ACURA), the California Institute of Technology and the University of California. This work was supported as well by the Gordon and Betty Moore Foundation, the Canada Foundation for Innovation, the Ontario Ministry of Research and Innovation, the National Research Council of Canada, and the U.S. National Science Foundation.

APPENDIX

TMT modeling venting strategy relies on pre-calculated look-up tables of wind reduction factors for various orientations and external wind speeds. Figure A1 presents a study of the wind reduction factors above M1 as a function of the venting area used. Four cases with the same orientation and reference wind speed were investigated for 0% (fully closed), 25%, 50% and 100 (fully open) vent area. All vents were open by the same amount. It appears that there is a linear relationship between the wind reduction factor and the vent area used. Thus the air velocity above M1 can be estimated by applying the formula

$$U_{M1} = fcU_o + b(fo - fc)U_o,$$

where U_o is the external wind speed, fc and fo are the reduction factors on M1 for fully closed and fully open vents respectively and b is a venting coefficient between 0 (closed vents) and 1 (open vents) (ex. 0.3 for 30% open vents). A control wind speed for M1 U_C can then be set, which will not be achieved when $fcU_o > U_C$ or $foU_o < U_C$ (see also [8]).

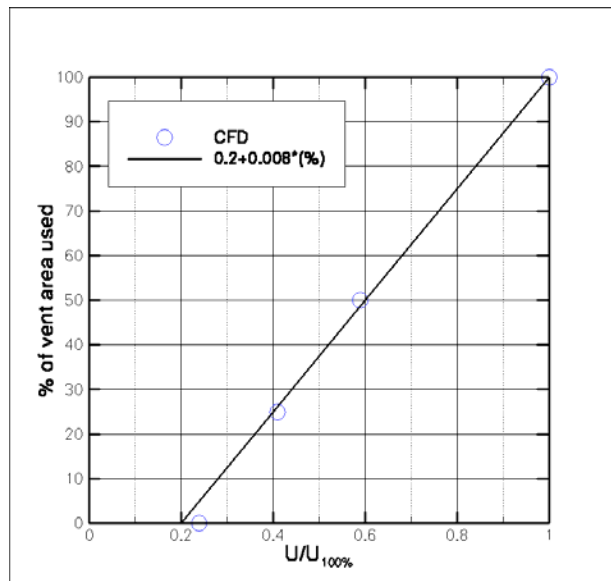


Figure A1. Wind speed on M1 normalized by wind speed at maximum vent opening as a function of vent opening, $z_a=30^\circ$, $z_z=25^\circ$, 5m/s

REFERENCES

1. De Young, D. S., Vogiatzis, K., "Numerical Simulations of Airflow in Very Large Telescope Enclosures", SPIE 5382-44, Baekaskog Sweden, 2003.
2. MacMynowski, D. G., K. Vogiatzis, K., Angeli, G. Z., Fitzsimmons, J., Nelson, E. J., "Wind Loads on Ground-Based Telescopes", Journal for Applied Optics, vol. 45, no 30, pp. 7912-7923, 2006.
3. Vogiatzis, K., & Angeli, G. Z., "Strategies for Estimating Mirror and Dome Seeing for TMT", SPIE 6271-27, Astronomical Telescopes and Instrumentation conference, Orlando, FL, May 24-31, 2006.

4. Vogiatzis, K., Angeli, G. Z., “Monte Carlo Simulation Framework for TMT”, SPIE 7017-29, Marseilles France, 2008.
5. Angeli, G. Z., Roberts, S., “Systems engineering for the preliminary design of the Thirty Meter Telescope”, SPIE 7017-3, Marseilles France, 2008.
6. Schöck, M. et al, “Status of the Thirty Meter Telescope site selection program”, SPIE 7012-68, Marseilles France, 2008.
7. Cho, M., Corredor, A., Pootrakul, S., Vogiatzis, K., “Thermal performance prediction of the TMT optics”, SPIE 7017-43, Marseilles France, 2008.
8. MacMynowski, D. G., Blaurock, C., Angeli, G. Z., “Dynamic analysis of TMT”, SPIE 7017-31, Marseilles France, 2008.
9. Pazder, J., Vogiatzis, K., “Dome and mirror seeing estimates for the Thirty Meter Telescope”, SPIE 7017-26, Marseilles France, 2008.
10. Sagals, G., MacMynowski, D. G., Vogiatzis, K., “Finite Element Analysis of TMT vibrations transmitted through telescope-enclosure-soil interaction”, SPIE 7017-73, Marseilles France, 2008.